Scanning Tunneling Spectroscopy on Single Crystal MgB_2

M. R. Eskildsen [a,1], M. Kugler [a], G. Levy [a], S. Tanaka [a,b], J. Jun [c], S. M. Kazakov [c], J. Karpinski [c], Ø. Fischer [a]

[a] *DPMC, University of Geneva, Switzerland*

[b] *Kansai Advanced Research Center, Communications Research Laboratory, Japan*

[c] *Solid State Physics Laboratory, ETH Zürich, Switzerland*

Abstract

We report on the results of scanning tunneling spectroscopy measurements on single crystals of MgB_2. Tunneling was performed both parallel and perpendicular to the crystalline c-axis. In the first case, a single superconducting gap ($\Delta_\pi = 2.2$ meV) associated with the π-band is observed. Tunneling parallel to the ab-plane reveals an additional, larger gap ($\Delta_\sigma \sim 7$ meV) originating in the highly two-dimensional σ-band. Vortex imaging in the π-band was performed with the field and tunnel current parallel to the c-axis. The vortices have a large core size compared to estimates based on H_{c2}, and show an absence of localized states in the core. Furthermore, superconductivity between the vortices is rapidly suppressed by an applied field. A comparison to specific heat measurements is performed.

Key words: MgB_2, STS, vortex
PACS: 74.50.+r, 74.70.Ad, 74.60.Ec

1 Introduction

Since the first report of superconductivity with a remarkably high $T_c = 39$ K in magnesium diboride (MgB_2) only two years ago [1], enormous progress has been made in the studies of this material. From a fundamental point of view, a central issue has been to establish that MgB_2 is a two-gap superconductor

[1] Corresponding author, address: DPMC, Université de Genève, 24 quai E.-Ansermet, CH-1211 Genève 4, Switzerland. Fax: +41 22 702 68 69. E-mail: morten.eskildsen@physics.unige.ch

- a concept which was introduced already in the fifties [2,3], and which has now found renewed relevance. Two-gap superconductivity in MgB_2 was first predicted theoretically [4] and is now commonly accepted, confirmed by a large number of experiments [5,6,7,8,9,10,11,12].

The two gaps in MgB_2 are associated with different parts of the Fermi surface, which is composed of 4 seperate sheets [4,13]. Two of these are coaxial cylindrical sheets parallel to c^*, derived from σ-antibonding states of the boron p_{xy} orbitals (σ-band). The other two sheets are derived from π-bonding and antibonding states of the boron p_z orbitals (π-band) and are three-dimensional. Calculations of the superconducting gap size for the two different bands yields $\Delta_\sigma \approx 7$ meV, and $\Delta_\pi = 1 - 3$ meV [14,15]. These values are respectively above and below what is expected for a BCS s-wave superconductor, $\Delta = 1.76\ k_{\rm B}T_{\rm c} = 5.9$ meV. Furthermore, and in contrast to many materials or alloys studied earlier, the two bands in MgB_2 have roughly equal weight, leading to new and interesting phenomena as we will show in the following. In this respect it has become clear, that local spectroscopic investigations of the mixed state is an ideal way to study the detailed nature of the superconducting state in MgB_2 at a microscopic level.

In this paper we summarize the present status of our scanning tunneling spectroscopy measurements, made possible by the recent availability of high quality MgB_2 single crystals. The results include spectra obtained by tunneling parallel as well as perpendicular to the crystalline c-axis, showing how the tunnel direction changes the coupling to the two bands. In addition, vortex imaging was performed with the tunnel current and magnetic field parallel to the c-axis. The vortices are found to have a number of remarkable properties: An absence of localized states, a very large vortex core size compared to the estimate based on H_{c2}, and a strong core overlap. Some of these results were reported earlier [16].

2 Experimental

The scanning tunneling spectroscopy (STS) experiments were performed using a home built scanning tunneling microscope (STM) installed in a ^{3}He, UHV cryostat containing a 14 T magnet [17]. The tunneling measurements were done using electrochemically etched iridium tips, with the bias voltage applied to the sample, i.e. a positive bias corresponds to probing the empty states and negative bias to the occupied states respectively above and below the Fermi level. A tunnel resistance of $R_{\rm t} = 0.2 - 0.4$ GΩ was used, and the differential conductance measured using a standard ac lock-in technique.

Single crystals of MgB_2 were grown using a high pressure method described

elsewhere [18], yielding platelike samples with the surface normal parallel to the crystalline c-axis. The surface area of the crystals are roughly 0.25×0.25 mm^2, and the thickness varies between a few up to ~ 100 microns. The critical temperature is typically $T_c = 37 - 38.6$ K, with a sharp transition, $\Delta T_c = 0.4 - 0.6$ K, measured by SQUID magnetometry [18]. Measurements were done both with the tunnel current, I_t, parallel and perpendicular to the c-axis. For $I_t \parallel c$, the spectroscopy was done on the surface of an as grown single crystal. In the case of $I_t \perp c$, a relatively thick crystal was cracked to expose a clean surface and immediately mounted and inserted into UHV.

The upper critical field of MgB_2 is highly anisotropic [19], with zero temperature extrapolations of respectively $H_{c2}^c = 3.1$ T and $H_{c2}^{ab} = 23$ T for single crystals [20], even though the latter value is subject to some uncertainty. Using the Ginzburg-Landau (GL) expression for $H_{c2} = \phi_0/(2\pi\xi^2)$, where $\phi_0 = h/2e$ is the flux quantum, yields an in-pane coherence length, $\xi_{GL}^{ab} = 10$ nm. Due to the large anisotropy, $\xi_{GL}^{c} = \xi_{GL}^{ab} \times H_{c2}^c/H_{c2}^{ab} \simeq 1 - 2$ nm. An estimate of the mean free path, based on the measured residual resistivity [21] and specific heat [11], and the calculated Fermi velocity [22], gives $l = 50 - 100$ nm, and a first estimate is thus that the samples are in the moderately clean limit [23]. However, the two-band nature of MgB_2 complicates the picture since H_{c2} is dominated by the two-dimensional σ-band which gives rise to the large H_{c2}-anisotropy, while the transport properties depends on both bands. A detailed analysis of the thermal conductivity by Solugubenko *et al.* concluded that the mean free path is roughly equal for the two bands with $l \approx 80$ nm [21].

3 Results

In the following we present the results of our measurements on MgB_2 single crystals.

3.1 Dependence on the tunnel current direction

The observation of a single or both superconducting gaps depends on the orientation of the sample, since tunneling along different directions changes the coupling to the two bands [22]. Roughly speaking, only bands with a component of the Fermi velocity parallel to the tunneling direction are observed. In particular, this means that coupling to the 2D σ-band is highly suppressed for tunneling parallel to the c-axis, whereas the 3D π-band will be probed for all tunneling directions.

In Fig. 1(a) we show a superconducting spectrum with $I_t \parallel c$. This is an average

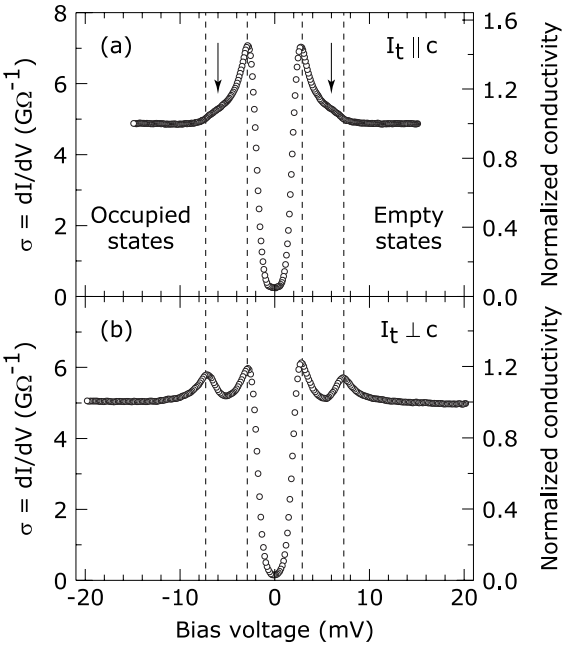

Fig. 1. Zero-field superconducting spectra of MgB_2 obtained by tunneling respectively parallel (a) and perpendicular (b) to the c-axis. In both cases $T = 0.3$ K and $R_t = 0.2$ GΩ ($U = 0.1$ V; $I = 0.5$ nA).

of 40 spectra obtained along a 100 nm path, which shows perfect homogeneity. One observes a single gap with coherence peaks at ± 2.9 meV associated with the π-band, and additional weak shoulders at ± 6 meV as indicated by the arrows. The shoulders are an admixture of the gap in the σ-band.

In Fig. 1(b) we show an average spectrum obtained for $I_t \perp c$. For this direction of tunneling, both superconducting gaps are present. The position of the low-energy coherence peak is unchanged as shown by the dashed lines. The additional peak arising from the σ-band is located at ± 7.3 meV. This is the first report of tunneling measurements on single crystals of MgB_2 for both $I_t \parallel c$ and $I_t \perp c$, which allows a direct correlation between the tunneling direction and the observed gap(s). Our results agree with those of Iavarone *et al.*, who investigated a number of single grains with different, but unknown absolute orientations [12].

For both tunneling directions the low zero bias conductance indicates a high quality tunnel junction and a low noise level. True vacuum tunneling conditions were confirmed by varying the tunnel resistance, R_t, and verifying that the spectra normalized to the conductance outside the superconducting gap collapse onto a single curve.

3.2 Temperature dependece for $I_t \parallel c$

Tunneling parallel to the c-axis, we measured the superconducting spectrum for a number of temperatures between 320 mK and 38.8 K. As discussed above this probes mainly the π-band. The results are presented in Fig. 2(a), and shows how the gap is gradually suppressed and finally closes at T_c. We have fitted the measured spectra to the conductance calculated using the BCS expression for the density of states, including a finite quasiparticle lifetime, Γ [24]:

$$N(\epsilon, \Gamma) = N_0 \left| \mathrm{Re} \frac{\epsilon - i\Gamma}{\sqrt{(\epsilon - i\Gamma)^2 - \Delta^2}} \right|. \quad (1)$$

The conductance is given by

$$\sigma(V) = \frac{dI}{dV} \propto \int d\epsilon \; N(\epsilon, \Gamma) \left(-\frac{\partial f(\epsilon + eV)}{\partial V} \right), \quad (2)$$

which we furthermore have convoluted by a Gaussian of width ω to take into account experimental broadening. The fits are shown in Fig. 2(a) and are found to be in good agreement with the measurements, except at low temperatures where the height of the coherence peaks is overestimated. The extracted values of the gap are shown in Fig. 2(b), yielding $\Delta_\pi(0) = 2.2 - 2.3$ meV. We find that $\Delta_\pi(T)$ is in excellent agreement with the temperature dependence of the BCS $\Delta(T)$ [25] when the zero temperature gap is scaled to 2.3 meV. The lifetime parameter $\Gamma = 0.1$ meV at low-T and increases with temperature. The experimental broadening $\omega = 0.5$ meV at base-T and increases only slightly to 0.8 meV at 10 K. For comparison the ac excitation used for the measurements was 0.4 meV RMS. Above 10 K the effects of Γ and ω becomes identical, and the latter is kept fixed.

3.3 Vortex imaging in the π-band

We now turn to measurements in an applied magnetic field. These measurements were done with $I_t \parallel \boldsymbol{H} \parallel c$, and hence selectively probes the π-band. In a type-II superconductor such as MgB_2, the magnetic field penetrates into the sample in the form of vortices each carrying one flux quantum, and generally arranged in a periodic array: the vortex lattice. In the core of each vortex, superconductivity is suppressed within a radius roughly given by the coherence length, ξ. The vortex spacing is determined by the applied field and the flux quantization, and in the case of a hexagonal vortex lattice it is $d = (2/\sqrt{3}\,\phi_0/H)^{1/2}$.

Necessary prerequisites for obtaining vortex lattice images is a high sample

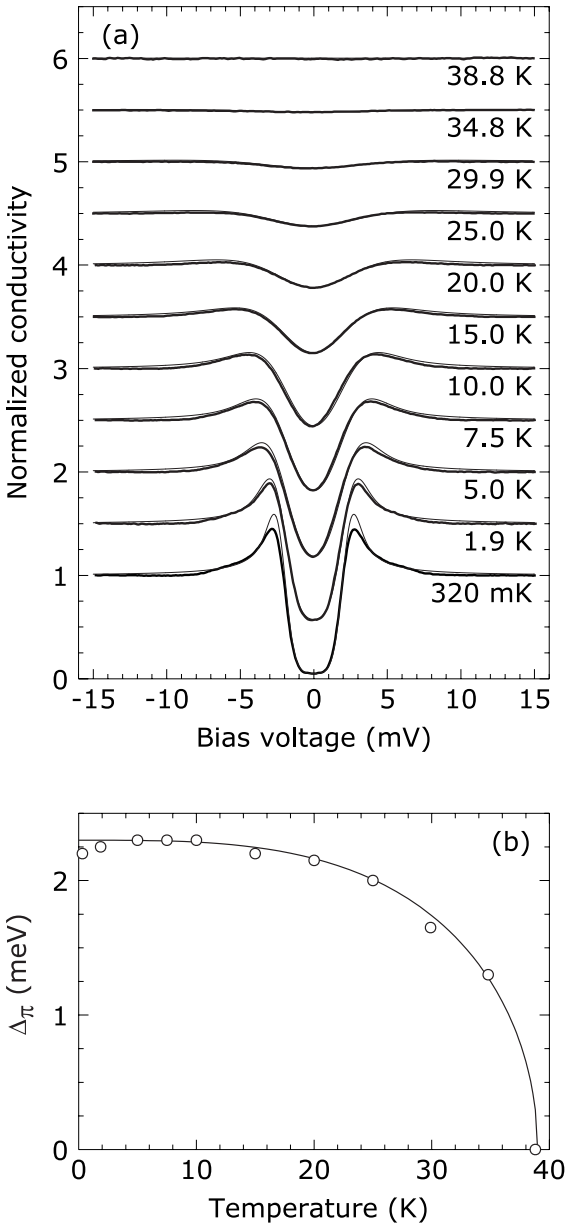

Fig. 2. (a) Spectra obtained a number of temperatures between 320 mK and 38.8 K (thick lines), tunneling parallel to the c-axis. Each spectrum is normalized to the conductance at 12 meV, and offset by 0.5 with respect to the previous one for clarity. The thin lines are our fits to the spectra as described in the text. (b) Temperature dependence of the superconducting gap in the π-band. The line is the BCS expression for $\Delta(0) = 2.3$ meV and $T_c = 39$ K [25].

homogeneity and a relatively flat sample surface. We verified that the first requirement is fulfilled by measuring perfectly reproducible spectra in zero field at a large number of positions along a several thousand ångstrøm line. A topographic STM image of the sample surface is shown in Fig. 3. The surface is seen to be very smooth, with an indication of a granular structure with a characteristic size of 5 - 10 nm. No effect of this "granularity" is observed in

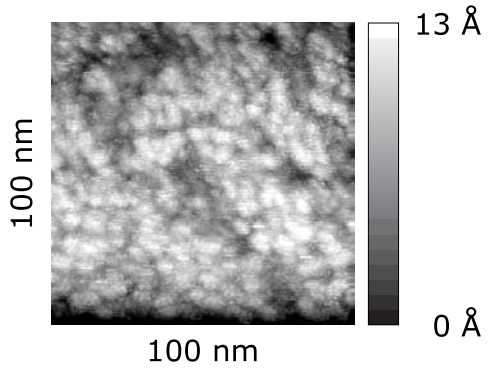

Fig. 3. STM topographic image of the as-grown surface of a MgB_2 crystal. The RMS roughness is 3 Å.

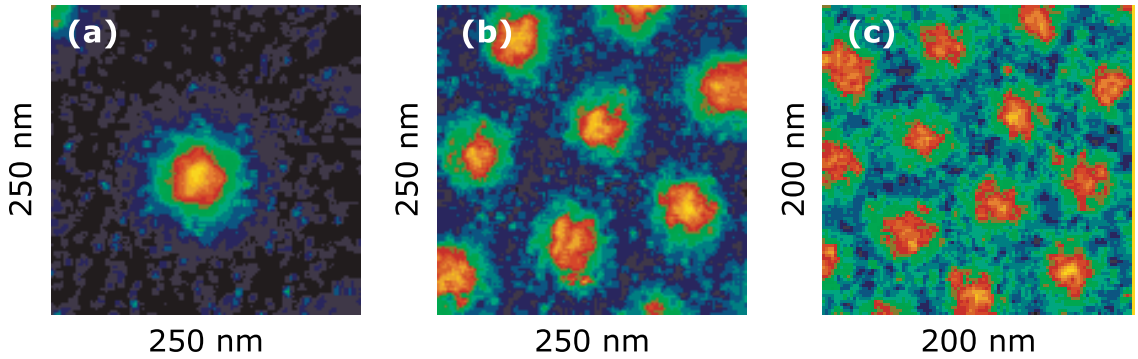

Fig. 4. (color) Vortices in MgB_2 at respectively 0.05 T(a), 0.2 T(b) and 0.5 T(c) at 2 K. The spatial variation of the conductance is shown by the color scale (different for each image).

the spectra.

The magnetic fields were applied at 2 K, and the system allowed to stabilize for at least a few hours. After this time no vortex motion was observed, indicating a fast relaxation and hence low vortex pinning in the crystal. In Fig. 4 we show STS images of vortices induced by three different applied fields. The images were obtained by measuring the differential conductance at zero bias. Low values of the conductance correpond to superconducting areas, and high values to the vortex cores. Figs. 4(b) and (c) show a well ordered hexagonal vortex lattice, with a lattice constant that corresponds to the applied field within 10%.

The low field in Fig. 4(a) is equivalent to a separation, $d = 220$ nm $\gg \xi_{GL}$. The vortices can therefore be considered as isolated from each other. Such isolated vortices are expected to contain localized quasiparticle states (Andreev bound states), which should show up as a zero bias conductance (ZBC) peak at the vortex centre [26,27], provided that the sample is sufficiently clean to prevent these from being smeared out by scattering. We have measured the evolution of the spectra at a large number of positions along a trace across the vortex

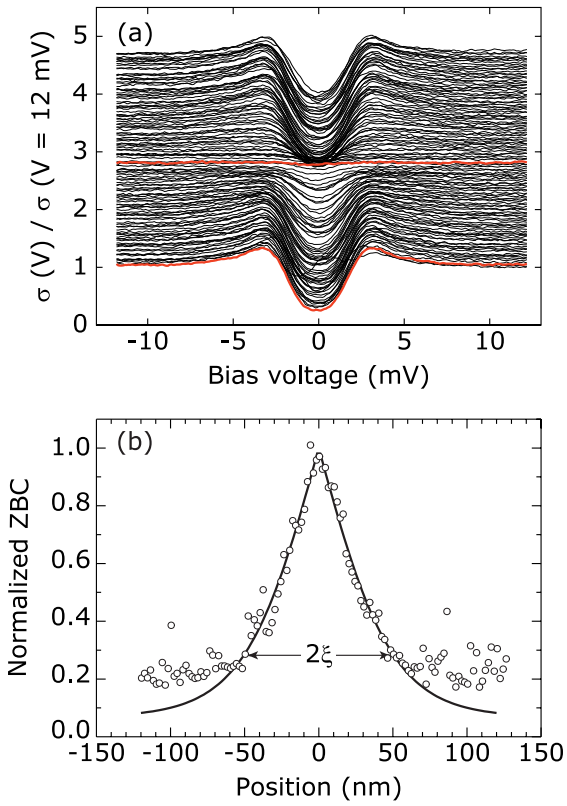

Fig. 5. (color) (a) 250 nm trace through the centre of the single vortex in Fig. 4(a), with spectra recorded each 2 nm. A spectrum at the vortex centre together with one far from the vortex core have been highlighted in red for clarity. (b) Normalized zero bias conductance versus distance from the centre. The line is a fit to eq. (3) in the text.

core. This is shown in Fig. 5(a). Contrary to expectations, we find that the normalized ZBC increases to one with no indication of any localized states. Instead, the spectra at the centre of the vortex are *absolutely flat*, with no excess spectral weight at or close to zero bias. This absence of localized states is striking, considering that $l = 5 - 10 \times \xi_{\rm GL}$. However, as we will show below, the coherence length in the π-band is approximately 50 nm. This is much larger than the GL estimate based on H_{c2}, and equal to only 1 – 2 times the mean free path. Nonetheless, for comparison systematic studies of $Nb_{1-x}Ta_xSe_2$ with $x = 0 - 0.2$, showed that even for $\xi/l \approx 1$ some excess weight close to zero bias was observed [27].

The spatial extent of the vortex is shown in Fig. 5(b), where we have plotted the normalized ZBC, $\sigma'(x, 0)$ from the vortex trace. It is immediately clear that the spatial extension of the vortex core is much larger than the 10 nm estimated from H_{c2}. We find that the vortex profile can be fitted by one minus the GL expression for the superconducting order parameter:

$$\sigma'(x, 0) = \sigma'_0 + (1 - \sigma'_0) \times (1 - \tanh x/\xi), \tag{3}$$

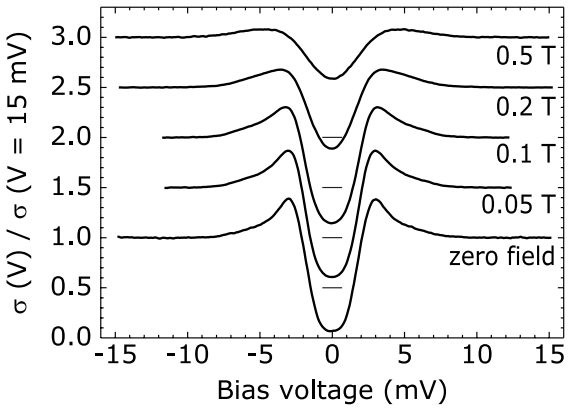

Fig. 6. Normalized spectra at 2K measured in zero field, and between the vortices for fields between 0.05 T and 0.5 T. Each subsequent spectrum is offset by 0.5 with respect to the previous one, with the bars at zero bias indicating the respective zero conductance.

where $\sigma_0' = 0.068$ is the normalized ZBC measured in zero field. The fit yields a coherence length, $\xi = \xi_\pi = 49.6 \pm 0.9$ nm. Using the GL expression to calculate the upper critical field with this value of the coherence length, yields $H_{c2}^{\pi} = 0.13$ T. This value is in strong contrast to the fact that we have performed vortex lattice imaging up to 0.5 T, and shows that a separate H_{c2} for the π-band does not exist.

The large ξ_π has however other consequences. In Fig. 6 we have plotted the normalized ZBC between the vortices. From this it is clear that even modest fields rapidly suppress superconductivity in the region between the vortices, seen both by an increase of the ZBC and by a suppression of the coherence peaks outside the vortex cores. This is consistent with earlier point contact spectroscopy measurements [6], with the addition that we resolve the local behaviour on a microscopic scale. Such a behaviour is only expected for fields close to H_{c2}, and corresponds to a significant core overlap.

4 Discussion

The vanishing of Δ_π at the bulk T_c and the sustained superconductivity despite a large vortex core overlap for $H > 0.2$ T leads to the conclusion that superconductivity in the π-band is induced by the σ-band, either by interband scattering, or Cooper pair tunneling [3,28]. This means that by itself the π-band would either be non-superconducting or have a very low T_c and upper critical field. Consequently the observed behaviour reflects the state in the σ-band by an interband proximity effect, along the lines of recent theoretical work [28]. This is also consistent with estimates of the coherence lengths, using the BCS expression $\xi_0 = \hbar v_F/(\pi\Delta(0))$ and considering each band separately.

Taking the calculated average Fermi velocity in the ab-plane for the π-band, $v_{\rm F}^{\pi} = 5.35 \times 10^5$ m/s [22], and the measured gap value $\Delta_{\pi}(0) = 2.2$ meV we get $\xi_0^{\pi} = 51$ nm, in excellent agreement with ξ_{π} obtained from the vortex profile. A similar analysis for the σ-band, using $v_{\rm F}^{\sigma} = 4.4 \times 10^5$ m/s [22] and $\Delta_{\sigma}(0) = 7.1$ meV [12] yields $\xi_0^{\sigma} = 13$ nm. This agrees with the coherence length obtained from $H_{\rm c2}$, and reinforces the conclusion that it is mainly the σ-band which is responsible for superconductivity in MgB_2, and thus determines the macroscopic parameters $T_{\rm c}$ and $H_{\rm c2}$. One must however bear in mind that this is a very simple-minded analysis. A detailed theoretical treatment of two weakly coupled superconducting bands in the presence of vortices, and the possibility of having have different coherence lengths, have to our knowledge not yet been presented.

4.1 Comparison to specific heat measurements

The vortex core overlap explains the strongly nonlinear field dependence of the electronic specific heat (T-linear term), γ [5,11]. In type-II superconductors core overlap is usually negligible, and in the simplest approximation each vortex creates the same number of quasiparticles at the Fermi surface, hence contributing by the same amount to the specific heat. In that case $\gamma = \gamma_{\rm n} \times H/H_{\rm c2}$, where $\gamma_{\rm n}$ is the electronic specific heat in the normal state. However, in the case of MgB_2, with strong core overlap in the π-band, the isolated vortex assumption is violated. Constructing a very simple model for the core overlap by

$$\sigma'(\boldsymbol{r}, 0) = \sigma_0' + (1 - \sigma_0') \times \left(1 - \Pi_i \tanh \frac{|\boldsymbol{r} - \boldsymbol{r}_i|}{\xi_{\pi}} \right), \qquad (4)$$

where $\boldsymbol{r}_i$ are the vortex positions for a hexagonal lattice with a density corresponding to the applied field, we can calculate the ZBC at any position in the vortex lattice unit cell. In Fig. 7 we compare the calculated conductance at the midpoint between three vortices with the measured "bulk" ZBC. This shows a very good agreement, especially taking into account that there are no free parameters in the calculation: ξ_{π} is determined from the vortex profile, and σ_0' is given by the finite ZBC in the zero field measurement. The π-band contribution to the specific heat can now be calculated by averaging the normalized ZBC in one vortex lattice unit cell, $\gamma_{\pi} = \gamma_{\rm n}^{\pi} \langle \sigma'(\boldsymbol{r}, 0) \rangle$ [28]. For this calculation we have set σ_0' equal to zero. On the other hand, the σ-band can be described by the usual linear field dependence $\gamma_{\sigma} = \gamma_{\rm n}^{\sigma} \times H/H_{\rm c2}$. Adding the terms gives $\gamma = \gamma_{\pi} + \gamma_{\sigma}$, where $\gamma_{\rm n}^{\pi}/\gamma_{\rm n}^{\sigma}$ is the relative weigth of the two bands. The calculated field dependence of γ is shown in Fig. 7, in perfect agreement with the measured specific heat for polycrystalline MgB_2[11], using $\gamma_{\rm n}^{\pi}/\gamma_{\rm n}^{\sigma} = 0.55/0.45$. The distribution of weight between the two bands is in agreement with other theoretical and experimental estimates [4,9,11,15,21]. Furthermore, the successful correlation with specific heat measurements makes us confident that

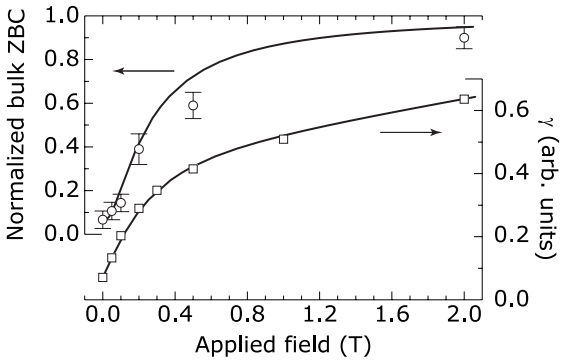

Fig. 7. Calculated "bulk" ZBC (left axis) and electronic specific heat, γ, for $\gamma_n^\pi/\gamma_n^\sigma = 0.55/0.45$ (right axis). The calculated values are compared to respectively the measured bulk ZBC (circles), and specific heat measurements on polycrystalline samples (squares) [11].

our results reflect bulk properties of MgB_2.

5 Summary

In summary, we have presented STS data on the π-band in MgB_2, including the first vortex imaging in this material. We have demonstrated the absence of localized states in the vortex core, a very large vortex core size and a strong core overlap. The data presents a striking experimental demonstration of the fundamentally different microscopic properties of the two bands in MgB_2.

Acknowledgements

We acknowledge valuable discussions and communication of data prior to publication with F. Bouquet, M. Iavarone, A. Junod and Y. Wang, and thank B. W. Hoogenboom and I. Maggio-Aprile for sharing their experience in STM/STS. This work was supported by Swiss National Science Foundation.

References

[1] J. Nagamatsu *et al.*, Nature **410**, (2001) 63.

[2] H. Suhl, B. T. Matthias and L. R. Walker, Phys. Rev. Lett. **3**, (1959) 552.

[3] For a review see G. Gladstone, M. A. Jensen and J. R. Schrieffer, in Superconductivity, edited by R. D. Parks, **2**, 665 (Marcel Dekker, New York, 1969).

[4] A. Y. Liu, I. I. Mazin and J. Kortus, Phys. Rev. Lett. **87**, (2001) 087005.

[5] Y. Wang, T. Plackowski and A. Junod, Physica C **355**, (2001) 179.

[6] P. Szabó *et al.*, Phys. Rev. Lett. **87**, (2001) 137005.

[7] X. K. Chen *et al.*, Phys. Rev. Lett. **87**, (2001) 157002.

[8] F. Giubileo *et al.*, Phys. Rev. Lett. **87**, (2001) 177008.

[9] F. Bouquet *et al.*, Europhys. Lett. **56**, (2001) 856.

[10] H. Schmidt *et al.*, Phys. Rev. Lett. **88**, (2002) 127002.

[11] A. Junod *et al.*, in *Studies of High Temperature Superconductors*, edited by A. Narlikar, **38**, 179 (Nova Publishers, Commack (N.Y.), 2002).

[12] M. Iavarone *et al.*, cond-mat/0203329 (to appear in Phys. Rev Lett.)

[13] J. Kortus *et al.*, Phys. Rev. Lett. **86**, (2001) 4656.

[14] A. A. Golubov *et al.*, J. Phys.: Condens. Matter **14**, 1353, 2002.

[15] H. J. Choi *et al.*, Nature **418**, 758 (2002).

[16] M. R. Eskildsen *et al.*, cond-mat/0207394 (to appear in Phys. Rev Lett.)

[17] M. Kugler *et al.*, Rev. Sci. Instrum. **71**, (2000) 1475.

[18] J. Karpinski *et al.*, cond-mat/0207263 (to appear in Supercon. Science and Tech.)

[19] S. L. Bud'ko, V. G. Kogan and P. C. Canfield, Phys. Rev. B **64** (2001) 180506; S. L. Bud'ko and P. C. Canfield, Phys. Rev. B **65** (2002) 212501.

[20] M. Angst *et al*, Phys. Rev. Lett. **88**, (2002) 167004.

[21] A. V. Sologubenko *et al.*, Phys. Rev. B **66**, 014504 (2002).

[22] A. Brinkman *et al.*, Phys. Rev. B **65** (2002) 180517.

[23] R. P. Huebener, Magnetic Flux Structures in Superconductors, 2nd ed. (Springer Verlag, Heidelberg, 2001).

[24] R. C. Dynes, V. Narayanamurti and J. P. Garno, Phys. Rev. Lett. **41**, (1978) 1509.

[25] B. Mühlschlegel, Zeitschrift für Physik **155** (1959) 313.

[26] H. F. Hess *et al.*, Phys. Rev. Lett. **62**, (1989) 214; F. Gygi and M. Schlüter, Phys. Rev. B **43**, (1991) 7609.

[27] Ch. Renner *et al.*, Phys. Rev. Lett. **67**, (1991) 1650.

[28] N. Nakai, M. Ichioka and K. Machida, J. Phys. Soc. Japan **71**, (2002) L23.